Proceedings of Global Power and Propulsion Society
ISSN-Nr: 2504-4400
GPPS Chania22
September 12 - 14, 2022
www.gpps.global

GPPS-TC-2022-0034

ON THE IMPACT OF FOULING ON THE STAGE INTERACTION IN A 2.5-STAGE COMPRESSOR

Daniel Kessler
Institute of Jet Propulsion and Turbomachinery
d.kessler@ifas.tu-braunschweig.de
Brunswick, Lower Saxony, Germany

Jens Friedrichs
Institute of Jet Propulsion and Turbomachinery
j.friedrichs@ifas.tu-braunschweig.de
Brunswick, Lower Saxony, Germany

Christian Werner-Spatz
Lufthansa Technik AG
christian.werner-spatz@lht.dlh.de
Hamburg, Hamburg, Germany

ABSTRACT

Jet engines and thus the compressor suffer operational, particle-based wear during their usage. The type of wear depends on the ambient conditions, the operating point, and the size of the particles. Fouling is one possible type of wear, consisting of the deposition of small particles on the blade's surface together with moisture from the air or leaked fluids of the compressor, thereby increasing the surface roughness and the blade thickness.

In order to better understand the effects of fouling, and especially the interaction of different affected compressor stages, investigations are carried out on a 2.5-stage test compressor to evaluate fouling in the compressor. Fouling is represented using a randomly distributed surface structure of hemispheres on both rotor rows. The roughness parameter Ra is based on surface measurements of a worn actual CFM-56 engine after operation. The results are compared to smooth rotor blades without coating. The effect on the compressor is evaluated by integral measurements of efficiency and pressure rise and by wake measurements with pneumatic 5-hole probes.

The results show integral losses in efficiency and pressure rise and, depending on the combination of rough rotor rows, a redistribution of the stage work. The second stage compensates for some of the losses of a rough first stage rotor, reducing the negative effects of the fouling.

INTRODUCTION

The efficiency of an aircraft engine is determined to a significant extent by the aerodynamic behavior of the high-pressure compressor during operation. Frictional surfaces and turbulences (i.e. secondary flows) forming in the sidewall regions are loss sources, which have an increased influence on the overall losses depending on the operating point. These loss sources are already known in the design process. Additionally, a compressor experiences operational wear during its lifetime, which leads to a deterioration of efficiency over the entire operating range. This wear depends on environmental conditions, the general operation, and the associated aging-related loads. Particles in the ambient air entering the gas path can lead to deterioration in performance. Typical examples of particles are aerosols, sand and dust, combustion products, and combustion residues. In addition, foreign bodies of the jet engine may also be present within the compressor. Thus, escaping oil, rust, and contaminated fuel can lead to erosion and deposits.

Depending on the particle size, temperature, and other factors, different effects like erosion or fouling can occur. Fouling describes the deposition of small particles combined with fluids on the compressor blades. The result of fouling is an increased surface roughness and a change of geometry. Both lead to increased losses and a change of the downstream flow.

In stationary gas turbines, filter systems reduce the number of particles that get into the compressor, resulting in only small particles (< 20 µm) in the gas path. According to Diankunchak, between 70 to 85 percent of efficiency degradation

in stationary gas turbines is due to fouling (Diankunchak, 1991). On jet engines, filters produce too high losses and cannot be used. Therefore, fouling cannot be avoided, but must be investigated to better understand its causes and effects.

A variety of studies have been performed in the past. Most of the measurements are performed on cascade wind tunnels (Brun et al., 2015; Igie et al., 2014; Kurz et al., 2016). It is easier to investigate the performance of a single, stationary blade. Rotating test rigs are used less often. Gbadebo et al. investigated a single-stage low-speed compressor (Gbadebo et al., 2004). Syverud and Bakken and Syverud et al. studied a full-scale engine. They showed a shifted operational area with the decreased mass flow and pressure rise. Their findings fit the results of Zaba (Syverud and Bakken, 2007; Syverud et al., 2007; Zaba, 1980). Seehausen et al. simulated the impact of hydraulic rough rows in a 10-stage high-pressure compressor. They fouled different rows based on the findings of Tarabrin et al. The simulation showed that a rough first stage has the greatest impact on the entire compressor. The reasons are disturbances that increase from stage to stage throughout the compressor (Seehausen et al., 2020; Tarabrin et al. (b), 1998). While there is literature on the effect of individually fouled stages on the entire compressor, the effect on neighboring stages has not been studied in detail.

EXPERIMENTAL SETUP

All measurements were carried out on the low-speed research compressor (LSRC) at the Institute of Jet Propulsion and Turbomachinery of the Braunschweig University. The test rig is an open tube test rig built to investigate highly loaded axial compressor stages. Air is drawn in through a standardized inlet nozzle. Via the pressure difference to the environment, the mass flow is determined. The fluid flows through the test section into a plenum box. The plenum box prevents upstream effects of the following downstream pipe system. A throttle and an auxiliary fan are installed in the pipe. The throttle and auxiliary fan allow the losses of the test rig to be changed and the mass flow to be freely adjusted. A detailed explanation of the test rig can be found in Achmus et al. (Achmus et al., 2019).

TEST SECTION

Figure 1 shows the 2.5-stage test section. The casing diameter is 600 mm and the hup-to-tip ratio is 0.75. The air flows from left to right. First, the air passes an inlet guide vane (IGV) which consists of 45 vanes. The IGV provides the pre-turning of the flow to achieve the required inflow conditions for the rotor. After the IGV, the air passes two stages which are designed as repeating stages, so the inflow flow angle and axial velocity profiles are similar for both stages. Both stages are identical regarding the blade geometry. Each rotor row consists of 43 blades and each cantilevered stator of 45 vanes. Both have a tip clearance of 1% relative to the channel height.

This test section is also used to perform investigations on bleed air extraction. Bleed air is taken through a gap in the casing downstream of the first stator. This gap was closed for the measurements in this paper to prevent interactions. However, this means that no measuring plane can be installed between the two stages.

The design mass flow is 6.82 kg/s with a design speed of 2800 rpm and a maximum Mach number of Ma = 0.28.

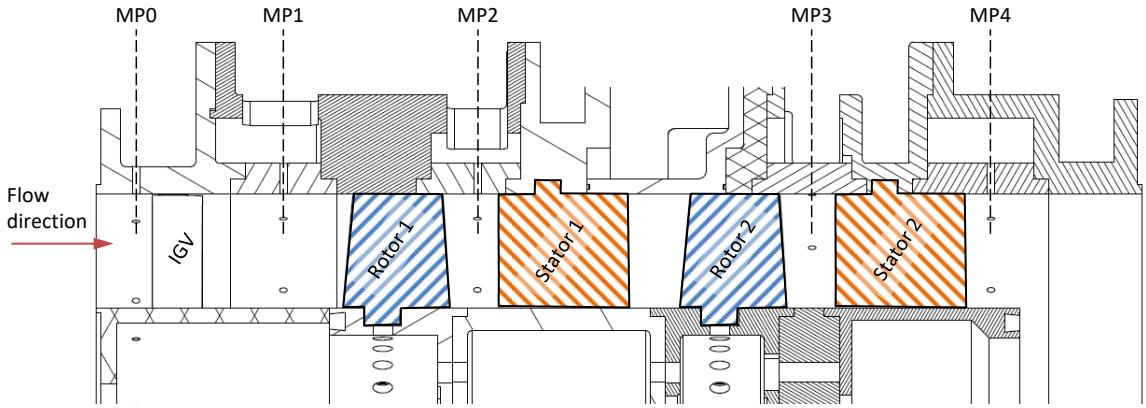

Figure 1 Cross Section of the 2.5 stage test section

REPRESENTATION OF FOULING

Early experimental representations of fouling use sandpaper as rough blade surface. Later studies used dissolved salts applied to the surface. When the solvent evaporates, a rough surface remains. In these studies, a metal-based coating was applied to the smooth blades. The Topocrom® coating consists of randomly distributed hemispheres that can be placed on top of each other, thereby depicting the random aspect of fouling. In the process, the roughness can be adjusted freely. However, coatings with higher roughness show more deviation over the surface area.

The roughness parameters are taken from real worn engine blades of a CFM-56. Several blades were examined by measuring the roughness using a laser/optical microscope at different points on the surface, and a representative patch

was selected. The roughness parameters (e.g. Ra = 2.5 µm) must be scaled to the low-speed case so that the boundary layer evolves similarly in both cases. The scaled arithmetical mean deviation is Ra = 11.5 µm. A more detailed explanation of the derivation of roughness can be found in Tolksdorf et al (Tolksdorf et al. 2021).

In the open literature, no general statement on the distribution of roughness in a compressor due to fouling, neither for the blades of a single-stage nor over several stages can be found. Tabarin et al. found that in the case of fouling, the deposits occur only before the first six stages, which was confirmed by Syverud et al. using salt deposits (Syverud et al., (2007); Tarabrin et al. (a), 1998). Suman et al. shows a uniform distribution over all stages (Suman et al. 2017). For the presented measurements, the complete rotor blade without the tip is fouled, representing an upper bound of wear. Only rotor blades were fouled. Stator rows, hub and shroud are smooth for all measurements.

After the application of the Topocrom coating, all blades were examined at multiple points on the surface. The coating is about 0.25 mm thick on each blade side, thickening the blade by 0.5 mm in total. An average roughness of Ra = 13 µm was measured in the center of the suction side. Compared to the Reynolds-like scaling, the surface is too rough. Accordingly, the results presented overestimate the real influence of fouling. In the direction of the leading edge, the roughness increases slightly. The selected coating process is not suitable for coating small radii. Accordingly, more material accumulates there, which was removed before the measurements. The decreasing roughness in the axial direction fits well with the results of Suman et al. Individual blades were measured in more detail. Individual roughness elements dominate the roughness at random locations of the blade. These individual rough elements can lead to a local transition of the boundary layer (Schreiber et al. 2002).

MEASUREMENTS

In these studies, a 2.5 stage axial compressor was investigated. In the different setups, the rotor of the first and second stage could be hydraulic smooth or rough, the latter representing a fouled blade. All blades of one rotor row are always completely smooth or fouled. All four possible combinations of smooth or rough rotors were investigated. The performance is evaluated based on characteristics and wake flow measurements in various measurement planes. The following chapters describe the measurement methods and error estimation techniques used.

STAGE CHARACTERISTICS

The integral stage performance is evaluated via pressure rise and efficiency. Due to the design of the test section, only the evaluation of the static quantities is possible. In every measuring plane (MP, see Figure 1), 19 static pressure holes are installed. The holes are evenly distributed and interconnected to average the pressure over the circumference. Thereby, the pressure rise of the entire test section and subsection can be calculated as:

$$\pi_{ss,ij} = \frac{p_{s,MPj}}{p_{s,MPi}}. \quad (1)$$

As stated in the description of the test section, it is not possible to measure the pressure between the two stages. The separation of the two stages has to be done between the rotor and stator of the first stage. Since only rough rotors are investigated, this division is still viable. With a torque flange in the shaft, the used power is measured for the efficiency calculation. Before the tests, the torque was measured without aerodynamic load at various speeds. The torque without load is subtracted from the measured value for each measurement to eliminate e.g. bearing losses. The torque can only be measured for the entire compressor. Therefore, only the entire test section efficiency can be calculated. The statistical error of the measurement is reduced by repeating the measurement (300 values for each point of the speed line) and arithmetically averaging them. It can be assumed that the measurement error results solely from the uncertainty of the pressure transducers.

All characteristic curves with the same speed start at the same corrected mass flow. The point of the characteristic, with the lowest mass flow, shows the last stable point at which a measurement can be made. The point is approached several times. The correted mass flow is defined as:

$$\dot{m}_{corr} = \dot{m} \bullet \sqrt{T_{amb} / 288.15K} \bullet 101325\,Pa / p_{amb}. \quad (2)$$

WAKE FLOW MEASUREMENTS

For a more detailed measurement, wake flow measurements are performed. For this, three five-hole probes (5HP) are installed in individual measuring planes. The probes are installed downstream of the IGV (MP1) and downstream of the rotor and stator of the second stage (MP3 and MP4). The probe downstream of the IGV is used to compare the different setups. The flow in this measurement plane is independent of the rest of the test section with no upstream effects of the first rotor.

The probes are moved by stepper motors in radial and circumferential direction. In the radial direction, 26 points are measured. The grid is denser in the boundary layer and becomes coarser in the center of the channel. In circumferential

direction, 25 angles are measured, with a total traversed angle of 8°, which corresponds to one stator passage. In total 650 points are measured for one wake flow measurement. At each point, 100 values are arithmetically averaged. Additionally to the traversing, the probe rotates on its axis to avoid high angular deviations.

All results shown below are measured at design mass flow and design speed.

UNCERTAINTIES

For the main flow parameters the following uncertainties have been calculated under design conditions:

Table 1: Calculated uncertainties of different flow parameters

	Symbol	Uncertainty
Inlet mass flow	$\dot{m}$	± 0.065 kg/s
Rotational speed	n	± 0.059 rpm
Static-to-static pressure ratio	π_{ss}	± 1.08E-04
Efficiency	η_{ss}	± 0.0097
Flow angle 5HP	β	± 0.2-0.8°

RESULTS AND DISCUSSION

Figure 2 shows the integral performance at different speeds and variations of smooth and rough rotors. Different colors indicate different speeds. The black curves correspond to 100% design speed (2800 rpm). A maximum of 105% (red) and a minimum of 70% (orange) design speed were measured. The setups of smooth and rough rotors are differentiated by different line patterns according to the line legend.

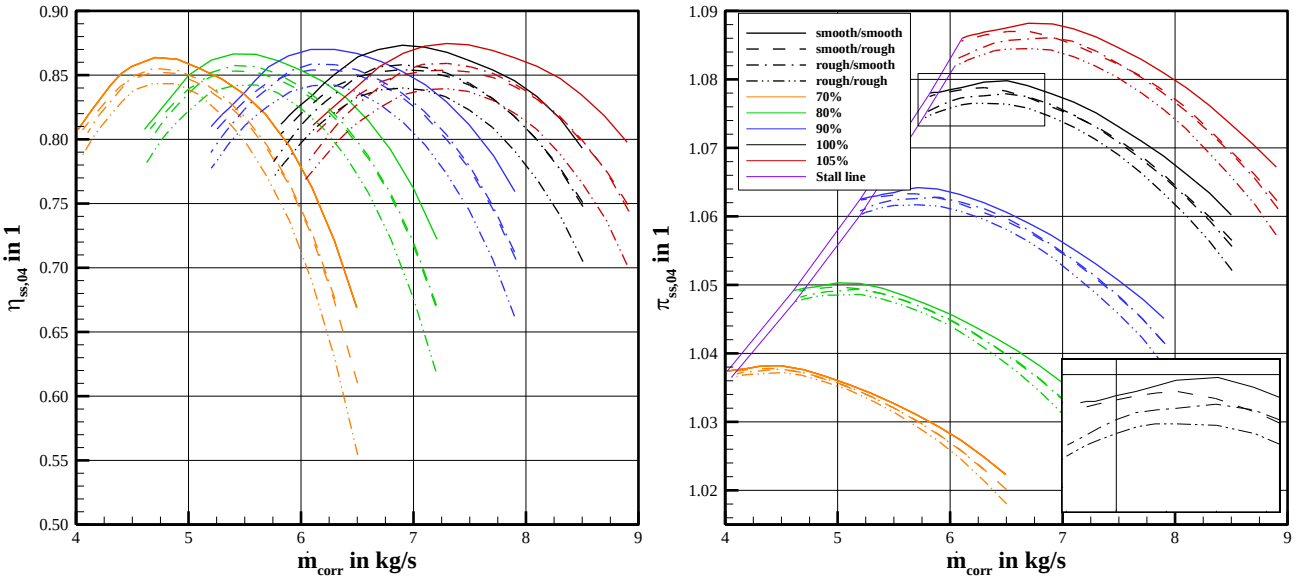

Figure 2 Static-to-static efficiency (left) and pressure rise (right) at various speeds and for different smooth and fouled setups

Comparing the characteristic curves of the fouled rotors to the smooth reference case (Figure 2 left), several effects can be found. The effects are in accordance with common findings in the literature. The compressor map is shifted to the left and down. The thickened boundary layers reduce the amount of fluid that passes the compressor for a given operating point, as well as the reduced passage area due to the thickened blade. Both static efficiency and pressure rise are reduced by the rough rotor blades. The operating range narrows on both sides. The stall line shifts towards larger mass flows. With rough rotors, the boundary layer is more stressed, and the secondary flow is more pronounced. Both lead to detachment, which causes the compressor to stall. For high mass flows, the narrowing of the operating range is not visible. All curves with the same speed start at the same mass flow since the throttle cannot be adjusted reproducibly. The auxiliary fan compensates for the additional losses at these points. At reduced speed, the effects due to the fouled blades also decrease. The blades are less loaded, and the boundary layers are less pronounced at lower mass flows.

The setups with only one rough rotor are equal over a wide operating range, indicating that it does not matter which of the two stages is fouled (smooth/rough; rough/smooth). The curves deviate only insignificantly from each other. Below the mass flow rate at design point, the two curves split. Toward stall, depending on which rotor is fouled, the two curves converge towards the extreme cases (smooth/smooth; rough/rough). It is deduced that in the throttled region, the first stage rotor has a stronger influence on the aerodynamics of the compressor than the following stage.

At design speed, the efficiency at the design point drops by about two percentage points with one rough rotor stage (Figure 2 left). The decrease in efficiency is independent of which of the two stages is fouled. With two rough rotor

stages, the efficiency decreases by about four percentage points relative to the smooth reference case. The torque and thereby the work done by the motor is approximately constant, which means that the loss of efficiency results mainly from the change in pressure rise. The pressure difference with one rough rotor decreases by about two percent. This effect is doubled with two rough stages to about a four percent lower pressure difference. The effects of the individual rough stages can therefore be roughly superimposed and result in a good approximation of the curve with two rough rotor stages.

Figure 3 shows the pressure rise of the individual stages, thus the work distribution can be evaluated. As mentioned, the splitting of the subsections cannot take place between the stages due to the test section geometry.

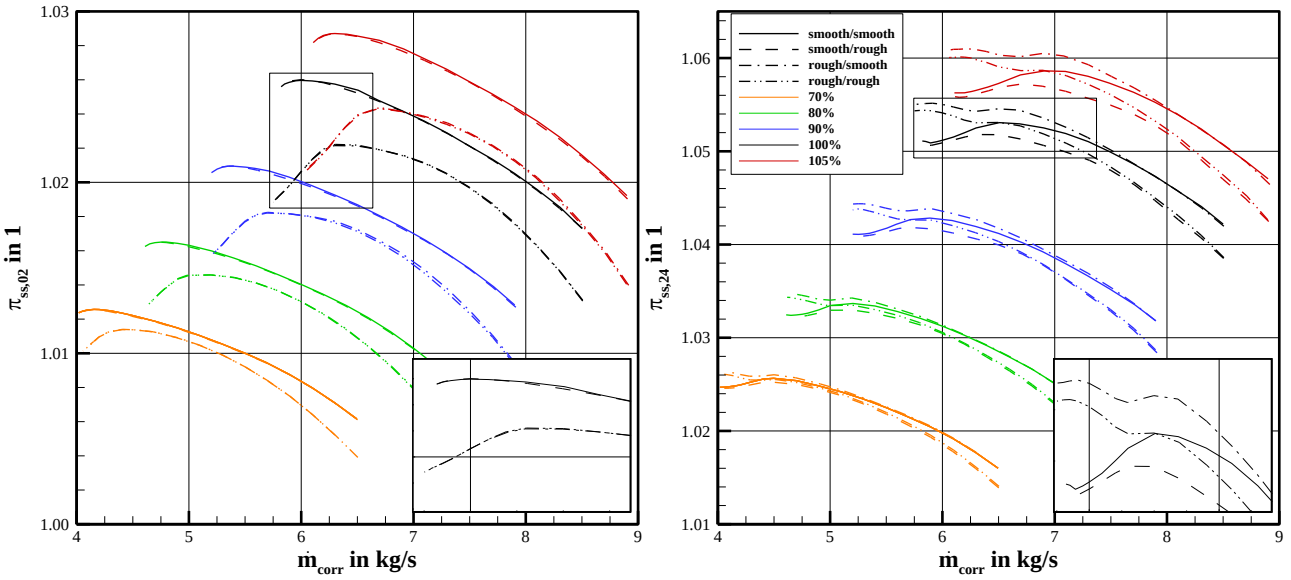

Figure 3 Stage pressure rise of IGV and rotor 1 (left) and stator 1 and stage 2 (right) at various speeds

The left side shows the pressure rise across IGV and rotor 1. The roughness of the second rotor has no upstream effect, so for these cases, the curves are identical. In contrast, the effect of a rough first rotor on the pressure rise is clearly visible. The pressure rise is significantly lowered over the entire operating range. At design speed and design mass flow, the pressure difference is lowered by about 10 percent compared to the smooth reference case. At further throttling, the pressure rise drops even further. The point of maximum pressure rise coincides well with the maximum pressure rise of the overall compressor. Due to the sharp drop in pressure rise caused by the rough rotor, the difference to the reference case increases to over 21 percent at 6.0 kg/s, confirming the statement that the first rotor is primarily responsible for the stall behavior.

The overall drop in pressure rise is not so pronounced for the entire test section due to the second stage. The subsection consists of two stators and a rotor. By considering static quantities, the pressure rise in this subsection is greater. At high mass flows, a dependence on the rotor can be seen again in this subsection. The curves with smooth or rough rotor 2 lie close to each other. However, the curves separate when the compressor is throttled. In the setups with a rough first rotor, the pressure rise increases faster than in the smooth case. At the stall point, the curves have not yet reached their maximum. The second subsection is still working stably at this point.

The rotor of the second stage partially compensates for the losses of a rough rotor in the first stage. The work within the stages is redistributed. As a result, a setup with a rough rotor can perform even better in the second stage than one with a smooth rotor. This effect may also result from the lowered pressure level at the beginning of the subsection. However, the same effect can also be observed in the pressure difference. In the case described above, near the stall limit with two rows of rough rotors, the pressure rise in the second subsection increases by about 5.5 percent. Due to the higher pressure ratio in this subsection, more than half of the pressure losses of the first subsection can be compensated. If only the rotor of the first stage is rough, the pressure difference within the second subsection even increases by 6.5 percent. Thus, more than 60 percent of the losses of the first stage are compensated.

Wake measurements are analyzed for a more detailed view of the impact of the rough surface on the flow in the channel. The results of the wake measurement downstream of the IGV show that there is no upstream effect of the roughened rotor blades on the IGV. The wake variables are independent of the measured combination of rough and smooth blades. Accordingly, only results from the wake of the second stage are shown in Figure 4. All measurements were performed at design speed.

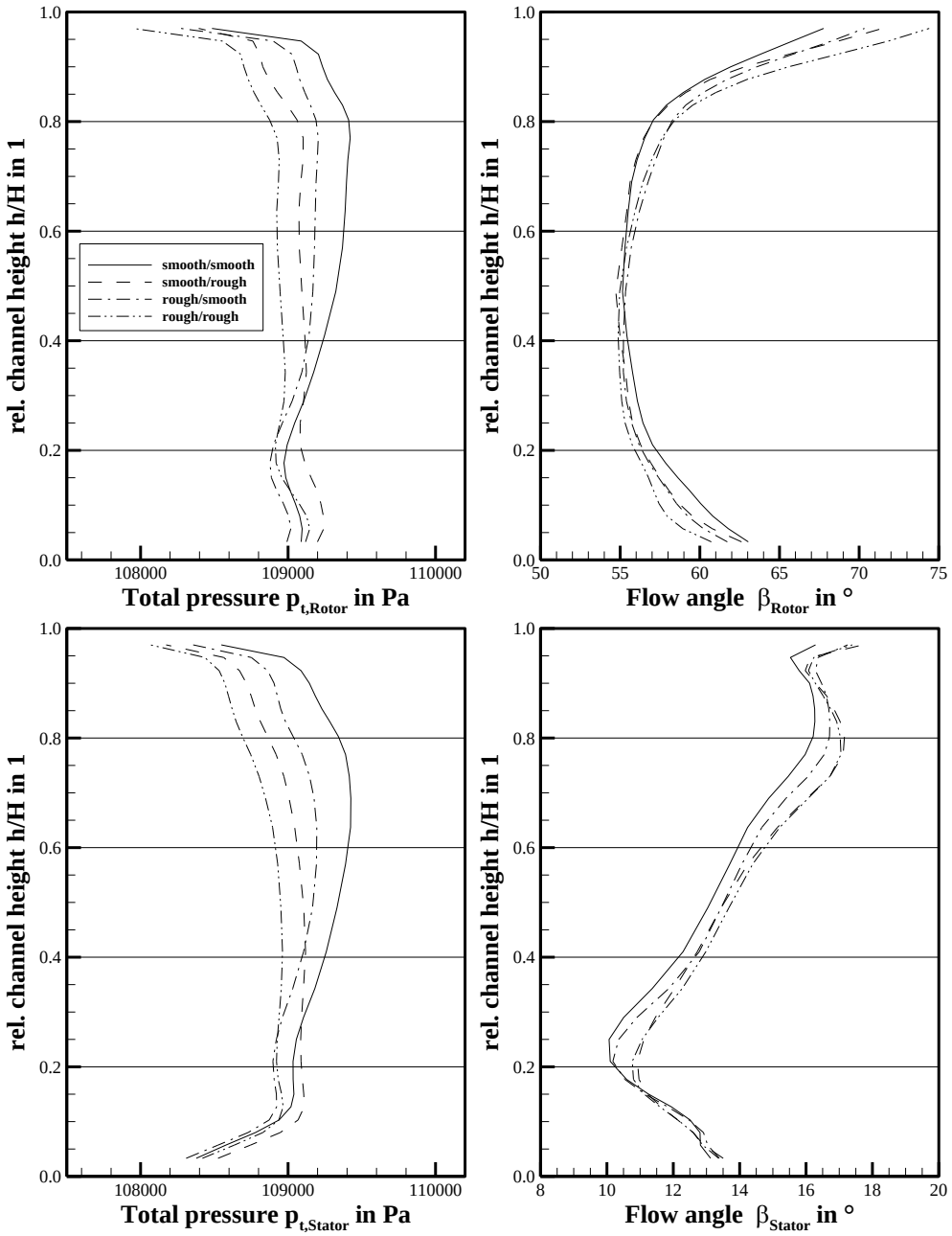

Figure 4 Circumferentially averaged wake flow measurements of total pressure (left) and flow angle (right) downstream of Rotor 2 in MP3 (top) and Stator 2 in MP4 (bottom) at design speed

Figure 4 (top left) shows the circumferentially averaged total pressure downstream of Rotor 2 versus the radial channel height. Over a large part of the channel height, total pressure losses are caused by the rough rotor blades. The losses are lower for a rough rotor directly upstream of the measurement plane than for a rough rotor in the first stage. The work redistribution between stages responds to a lower pressure rise of the first rotor. As a result, the total pressure for the rough/smooth (dash-dot) setup is higher than in the inversed case. The rough rotor blades influence the secondary flow. The influence of the tip gap vortex on the total pressure can be seen on the casing. The lower load on the rough blade results in a lower pressure difference on the blade's sides and thus in a weaker gap vortex. As a result, a slightly steeper gradient can be seen in the top five percent of the channel. However, the effect is very weak and is within the uncertainty of the measurement. The lower quarter of the canal shows a reverse effect compared to the middle of the canal. The setup with a rough rotor in the second stage (dashed) achieves a higher total pressure than the smooth reference case. At 20 percent channel height, the influence of corner separation can be seen. Here, the fluid flows around the trailing edge of the blade. Fluid with higher pressure flows from the pressure side into the low-energy boundary layer region on the suction side. The flow detaches at the point and generates total pressure losses. The region of corner separation is smaller for the setup mentioned. The rough surface of the blade forces a transition of the boundary layer. The turbulent boundary layer is more stable due to constant energy input by vortices. In addition, the pressure difference

between the two blade sides is reduced, as already mentioned for the tip gap. The changed secondary flow provides a higher total pressure in the area. Even if only the rotor of the first stage (dash-dot) has a rough surface, similar tendencies can be seen. The effects described occur in a similar form in the first stage. The positive influence on the total pressure mixes out and is less pronounced. However, the losses are lower than in the center of the channel. The setup with two rows of rough rotors combines the described effects and lies between the other two curves.

The downstream flow angle in the plane shows a redistribution of the flow to the hub (Figure 4 top right). The mass flow rate at the casing is reduced due to the thickening of the boundary layer. At the same time, more fluid can flow near the hub because the secondary flow is less severe. The different axial velocities induced by the changed mass flow and constant rotational speed result in different downstream flow angles. Underturning occurs in the lower half of the channel, while the downstream flow in the upper half of the channel shows overturning.

Downstream of the second stator, the same effects can still be seen in principle (Figure 4 bottom left). The misaligned flow through the rotor leads to further losses through the stator, especially in the upper third. However, the stator also reduces the false inflow. An increased angle in the downstream flow can still be seen from about 15% channel height. However, this is reduced to about 1° (Figure 4 bottom right). The lower deflection leads to lower static pressure in the measuring plane.

CONCLUSIONS

This paper aims to investigate the stage interaction in a 2.5-stage axial compressor with fouling. For this purpose, rotor blades were coated with a coating that realistically reproduces fouling in geometry and distribution. The roughness parameters were derived from real worn engine blades and scaled for the incompressible test case. Different setups with rough blades in one or both stages were investigated and compared against a smooth reference case. Integral performance of test section (static-to-static efficiency and pressure rise) and the stage performance were evaluated. Additional wake flow measurements in the second stage show the influence of the rough surfaces on the secondary flow in the channel.

The integral measurements show effects known from literature: Fouling reduces the operating range of the compressor. The compressor map shifts to the bottom left due to increased losses and thickening boundary layers. The efficiency decreases as a function of roughness by two percentage points with only one row of roughness and by about four percentage points if both rotors are fouled. In the setups with only one row of rough rotors, only minor differences can be seen over a wide range of the characteristic. Only at high load do the curves differ from each other and approach the extreme cases (both rotors smooth or rough). It can be shown that the first rotor is essential for behavior near the stall limit.

The division of the pressure rise between the stages shows that it is primarily the rotor contained in the first subsection that influences the performance. However, a redistribution of work can also be observed. A rough rotor in the first stage leads to heavy losses if throttled. The pressure difference across the subsection drops by over 20 percent. If the first stage does not perform, the second-stage rotor compensates for more than 50 percent of the losses increasing the pressure rise by up to six percent. As a result, the overall performance does not drop as much.

The total pressure wake shows the losses caused by fouling due to thicker boundary layers over a large part of the channel height. At the same time, the secondary flow is also affected. The gap vortex at the casing is less pronounced so that the losses decrease. In addition, the corner separation at the hub is suppressed. As a result, the curves intersect, and setups with a rough rotor in the second stage achieve better total pressure in the lower quarter of the channel. The flow is radially redistributed due to the changed secondary flow and the boundary layers. The resulting changed axial velocities lead to changed downstream flow angles. The stator can only partially reduce the misaligned flow and causes further losses above 15 percent channel height.

Future measurements are planned featuring a modified measuring section with an additional measurement plane between the stages. Thereby, the stage comparison will be improved, and additional insights are likely to be gathered. In addition, stator vanes have already been provided with the same coating as the rotors used to investigate different combinations of rough blades and vanes within the stage. Furthermore, measurements will be carried out with mixed rows consisting of smooth and rough blades.

REFERENCES

Achmus, M., Friedrichs, J. and Becker, B. (2019). *Experimental Investigation of the Flow Characteristics in a Circumferential Bleed Port Geometry and the Interaction with a 1.5-stage Axial Compressor*. Proceedings of International Gas Turbine Congress (IGTC-2019-149), Tokyo, Japan.

Brun, K., Foiles, W. C., Grimley, T. A. and Kurz, R. (2015). *Experimental Evaluation of the Effectiveness of Online Water-Washing in Gas Turbine Compressors*. Journal of Engineering for Gas Turbines and Power, Vol. 137 Issue 4. DOI: 10.1115/1.4028618

Diakunchak, I. S. (1991). *Performance Deterioration in Industrial Gas Turbines*. Journal of Engineering for Gas Turbines and Power, Vol. 114 Issue 2. DOI: 10.1115/1.2906565.

Gbadebo, S. A., Hynes, A. and Cumpsty, N. A. (2004). *Influence of Surface Roughness on Three-Dimensional Seperation in Axial Compressors*. Journal of Turbomachinery, Vol. 126, Issue 4. DOI:10.1115/1.1791281

Igie, U., Pilidis, P., Fouflias, D., Ramsden, K. and Laskaridis, P. (2014). *Industrial Gas Turbine Performance: Compressor Fouling and On-Line Washing*. Journal of Turbomachinery, Vol. 136, Issue 10. DOI: 10.1115/1.4027747

Kurz, R., Musgrove, G. and Brun, K. (2016). *Experimental Evaluation of Compressor Blade Fouling*. Proceedings of ASME Turbo Expo 2016, GT2016-56027. DOI: 10.115/GT2016-56027

Schreiber, H.-A., Steinert, W. and Kuśters, B. (2002). *Effects of Reynolds Number and Free-Stream Turbulence on Boundary Layer Transition in a Compressor Cascade*. Journal of Turbomachinery. DOI: 10.1115/1.1413471

Seehausen, H., Gilge, P., Kellersmann, A., Friedrichs, J. and Herbst, F. (2020). *Numerical Study of Stage Roughness Variations in a High Pressure Compressor*. International Journal of Gas Turbine. DOI: 10.38036/jgpp.11.3_16

Suman, A., Morini, M., Aldi, N., Casari, N., Pinelli, M. and Spina, P. R. (2017). *A Compressor Fouling Review Based on an Historical Survey of ASME Turbo Expo Papers*. Journal of Turbomachinery Vol. 139, Issue 4. DOI:10.1115/1.4035070

Syverud, E. and Brekke, O (2007). *Online Water Wash Tests of GE J85-13*. Journal of Turbomachinery Vol. 129, Issue 1. DOI: 10.1115/1.2372768

Syverud, E., Brekke, O. and Bakken, L. E. (2007). *Axial Compressor Deterioration caused by Saltwater Ingestion*. Journal of Turbomachinery, Vol. 129, Issue 1. DOI:10.1115/1.2219763

Tarabrin, A. P., Schurovsky, V. A., Bodrov, A. I. and Stalder, J.-P. (1998*). An Analysis of Axial Compressor Fouling and a Blade Cleaning Method*. Journal of Turbomachinery, Vol. 120, Issue 2. DOI:10.1115/1.2841400

Tarabrin, A. P., Schurovsky, V. A., Bodrov, A. I. and Stalder, J.-P. (1998*). Influence of Axial Compressor Fouling on Gas Turbine Unit Perfomance Based on Different Schemes and With Different Initial Parameters*. Proceedings of ASME Turbo Expo 1998, 98-GT-416. DOI: 10.1115/98-GT-416

Influence of roughness on the transition modeling in compressor flows. Proceedings of ASME Turbo Expo 2021, GT2021-60003. DOI: 10.1115/GT2021-60003

Zaba, T. (1981). *Losses in Gas Turbines due to Deposits on the Leading Edge*. Brown, Boveri & Cie, Publication No. CH-T 113433E

NOMENCLATURE

Symbols

h/H	Relative channel height
ṁ	Mass flow
n	Rotational speed
p	Pressure
R	Radius
T	Temperature
β	Flow angle
η	Efficiency
π	Pressure ratio

Subscripts

0,1,2,3,4	Measurement Plane 0 to 4
amb	Ambient
corr	Corrected
i,j	Couting variable
is	Isentropic
ref	Reference
s	Static
ss	Static to static
t	Total

ACKNOWLEDGMENTS

The authors would like to thank Stefan Kuntzak from Lufthansa Technik, Dr. Andreas Gantner, and Guido Döbbener from ANSYS Germany, and the Alexander Hergt from DLR Cologne are gratefully acknowledged for helpful discussions within the ProTherm project. The work reported here is supported by the German Federal Ministry for Economic Affairs and Climate Action as part of the LuFo V-3 program, under grant number 20X1706.